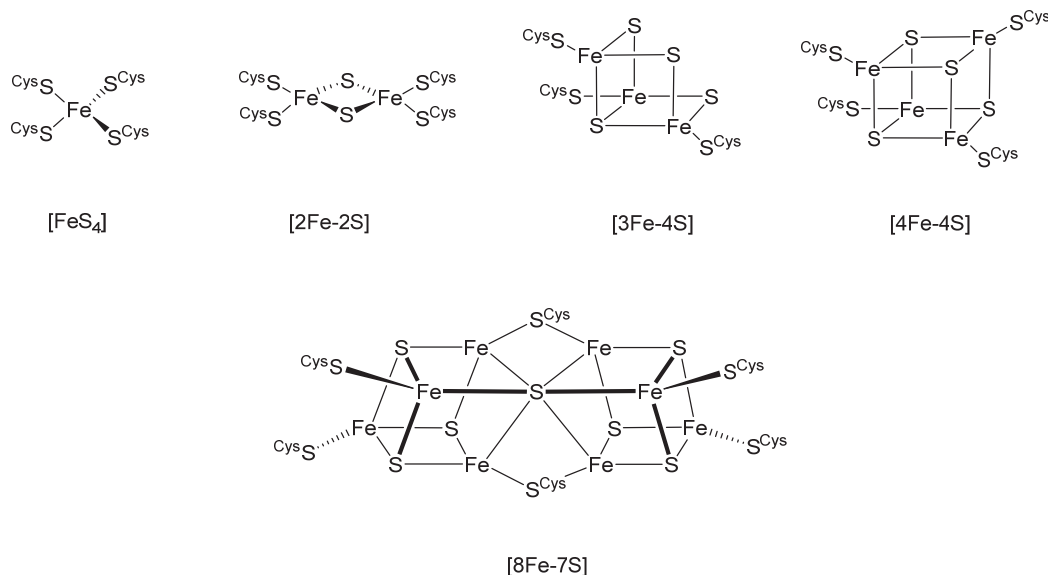


# 1 Introduction

## 1.1 Iron Sulfur Clusters in Nature

Iron sulfur clusters are ubiquitous cofactors, which exist in a variety of forms and serve a multitude of functions including electron transport, redox reactions and sensing.<sup>[1,2]</sup> They are thought to be among the oldest cofactors and are certainly among the most versatile ones.<sup>[2-5]</sup> They may even have been involved in the early evolution of life, which is supposed to have developed on the surface of iron sulfur structures.<sup>[6]</sup> They were first discovered by Beinert and Holm in 1960 using EPR spectroscopy, and since then a multitude of iron sulfur clusters have been discovered in all three kingdoms of life.<sup>[7]</sup> The most widespread forms include [2Fe-2S] clusters and [4Fe-4S] clusters but mononuclear species (rubredoxines) as well as [3Fe-4S] clusters and larger clusters exist as well, including the [8Fe-7S] P-Cluster and FeMoco found in nitrogenase (Figure 1.1).<sup>[1,8-11]</sup> Due to antiferromagnetic coupling between the two tetrahedrally coordinated iron centers, [2Fe-2S] clusters are typically found in an  $S = 0$  ground state in their diferric form.<sup>[12,13]</sup> In [4Fe-4S] cluster, two pairs of ferromagnetically  $\text{Fe}^{\text{III}}\text{Fe}^{\text{II}}$  subunits are antiferromagnetically coupled, resulting in a total  $S = 0$  ground state for the  $\text{Fe}^{\text{III}}_2\text{Fe}^{\text{II}}_2$  form.<sup>[1,12,14,15]</sup>



**Figure 1.1:** Different structural motifs found for biologically relevant iron sulfur clusters.

Due to the relatively easy accessibility of both the ferrous and ferric oxidation state, iron sulfur clusters are often involved in electron transfer processes, in which their redox potential spans a range from  $-600$  mV to  $+400$  mV, depending on cluster size, ligands, and the

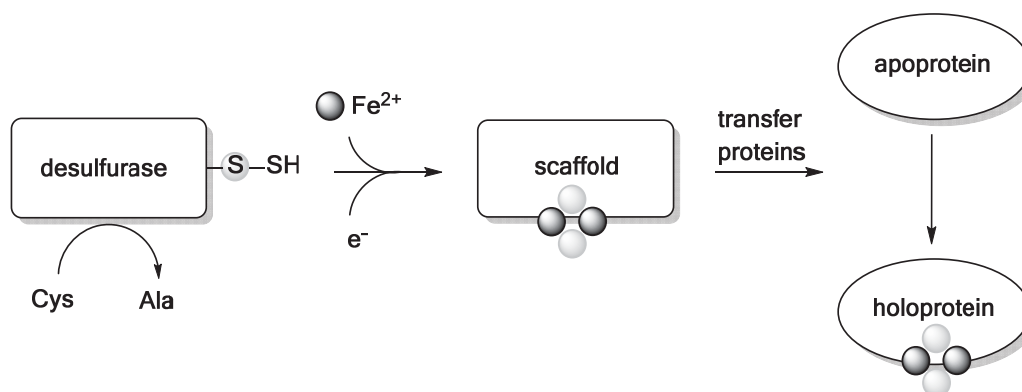


environment in the respective protein. The highest potentials are found in HiPIPs (high potential iron sulfur proteins) [4Fe–4S] clusters, which utilize the [4Fe–4S]<sup>2+/3+</sup> couple rather than the [4Fe–4S]<sup>1+/2+</sup> couple, and in [2Fe–2S] Rieske clusters, which feature two terminal histidine ligands instead of the commonly found cysteine ligands.<sup>[16–19]</sup> Iron sulfur cofactors have also been found in a number of different roles, highlighting their versatility: They are essential in catalytic transformations such as the transformation of citrate into isocitrate carried out by aconitase in the citrate cycle.<sup>[20]</sup> In this process, a non-protein coordinated iron ion of a [4Fe–4S] cluster offers a free coordination site and acts as a Lewis acid in the activation of water. Iron sulfur clusters have also been found to act as sensors for small molecules such as dioxygen or nitric oxide or for cellular conditions such as iron content or oxidative stress.<sup>[21–24]</sup> Roles of iron sulfur proteins in DNA replication and repair and thiolation of RNA have also been reported in recent years.<sup>[25–28]</sup> Additionally, iron sulfur cofactors play important roles in mediating proton coupled electron transfer (PCET) reactions, which will be explored in more detail in chapter 1.4.<sup>[29]</sup> A special role of iron sulfur cofactors as initiators and substrates of radical reactions has been described for radical SAM enzymes, which will be the focus of chapter 1.5.<sup>[30]</sup>

## 1.2 Iron Sulfur Cluster Biogenesis

Since iron sulfur clusters play important roles in a variety of biological processes, iron sulfur cluster biogenesis is an essential process in all three kingdoms of life. Defects in this process are associated with various diseases including Friedreich ataxia and IscU myopathy.<sup>[31–34]</sup> Although iron sulfur clusters can be reconstituted *in vitro* by addition of S<sup>2-</sup> and Fe<sup>3+</sup> to the respective apoproteins,<sup>[35]</sup> iron sulfur complex formation and maturation *in vivo* follows a more complex and closely regulated mechanism.<sup>[36,37]</sup> Three distinct machineries for iron sulfur cluster biogenesis exist (NIF, ISC, SUF).<sup>[31]</sup> The ISC and SUF systems are responsible for the generation and maturation of iron sulfur clusters under normal and stress conditions, respectively<sup>[38–40]</sup> whereas the NIF system carries out the maturation of nitrogenase in azototrophic bacteria. Although they operate under different conditions, the ISC and SUF systems follow a similar mechanism (Scheme 1.1). Cysteine desulfurase has been identified as the source of the sulfides in this process, which provides the sulfide needed in Fe/S cluster assembly by generating a persulfide intermediate *via* conversion of cysteine to alanine.<sup>[41]</sup> For this process an electron donor such as a ferredoxin reductase is necessary to achieve the reduction from S<sup>0</sup> to S<sup>2-</sup>.<sup>[42]</sup> Since free iron ions are cytotoxic, they must be delivered by iron donors such as the iron binding protein frataxin (in bacterial CyaY and mitochondrial Yfh1) of the ISC system.<sup>[43–45]</sup> [2Fe–2S] clusters can then be assembled on scaffold proteins such as the bacterial IscU, which contain three conserved iron sulfur cluster binding cysteine residues.<sup>[42,46,47]</sup> The thus assembled cluster can subsequently be transferred to the respective apoproteins. The transfer proteins needed in this last step must induce dissociation of the

cluster from the scaffold protein and ensure accurate transfer to the respective position in the apoprotein.<sup>[48,49]</sup> It has been shown that the scaffold protein IscU changes its conformation to facilitate release of the formed iron sulfur cluster.<sup>[50]</sup> The formation of larger clusters such as [4Fe–4S] clusters is achieved by fusion of two [2Fe–2S] clusters and is believed to require an additional reductant.<sup>[51,52]</sup> This overall principle of iron sulfur cluster biogenesis seems to be conserved in prokaryotes and eukaryotes reaching from yeast to human cells.<sup>[53–57]</sup>



**Scheme 1.1:** Overview of different steps occurring in iron sulfur cluster biogenesis, scheme modified from literature.<sup>[31]</sup>

*In vivo* and *in vitro* studies have already provided valuable insight into the cluster transfer during iron sulfur cluster biogenesis but there is only limited understanding of this process on a molecular level. Transfer of intact [2Fe–2S] clusters from the IscU protein to the target apoprotein was shown to be ATP dependent and to proceed under second order kinetics. It was proposed that cluster transfer might occur *via* successive ligand exchange after formation of a transient donor-acceptor complex, since a conserved aspartate residue Asp39 in *azotobacter vinelandinii* IscU plays a crucial role in facilitating cluster release.<sup>[58]</sup> Initial displacement of this residue and subsequent coordination of the cysteine residue of the respective apoprotein was proposed to occur as a rate determining step in cluster transfer. Additionally, chaperone and co-chaperone complexes of the scaffold and target protein need to be present during the iron sulfur cluster transfer process.<sup>[59–61]</sup> However, detailed mechanistic studies of ligand exchange and rearrangement at the [2Fe–2S] core are needed to fully understand this essential process on a molecular level.

### 1.3 Marcus Theory and Proton Coupled Electron Transfer

In 1975 Marcus and Sutin presented a theory for treating the thermodynamics of electron transfer reactions that is still widely applied today and referred to as Marcus theory.<sup>[62,63]</sup> The free energy barrier  $\Delta G^\ddagger$  for an electron transfer can be calculated from the difference in free energy of the educt and product  $\Delta G^\circ$  and the reorganization energy  $\lambda$ :

$$\Delta G = 1/4 \lambda (1 + \Delta G^\circ/\lambda)^2$$

The rate  $k_{ET}$  of the electron transfer at a temperature  $T$  is then determined as ( $k_B = 1.38 \cdot 10^{-23} \text{ J K}^{-1}$ ,  $h = 6.626 \cdot 10^{-34} \text{ J s}$ , the pre-exponential frequency factor  $\kappa$  contains the probability of crossing from one energy surface to the other and depends of the degree of adiabaticity and the general nature of the electron transfer):

$$k_{ET} = (\kappa k_B T/h) \exp(-\Delta G/k_B T)$$

Thus, according to Marcus Theory, the rate of an electron transfer step mainly depends on the following three factors: The reorganization energy  $\lambda$  is associated with geometrical changes both at the actual redox center (inner-sphere reorganization energy,  $\lambda_{\text{inner}}$ ) as well as of the surrounding protein and solvent molecules (outer-sphere reorganization energy,  $\lambda_{\text{outer}}$ ). It has to be rather small to enable efficient electron transfer since a larger reorganization energy leads to a larger activation free energy  $\Delta G^\ddagger$ . Additionally, the slope of the two parabolas of the free energy surface of both educts and products must not be too steep, since this would lead to a large  $\Delta G^\ddagger$ . Finally, the difference in free energy  $\Delta G^\circ$  between the educt and the product determines the rate of the electron transfer.  $\Delta G^\ddagger$  decreases with increasing  $\Delta G^\circ$ . A maximum rate is reached when  $\Delta G^\circ = -\lambda$  and the reaction then proceeds activationless. Upon further increase of  $\Delta G^\circ$  (*i.e.* when  $\Delta G^\circ > \lambda$ )  $\Delta G^\ddagger$  increases as well, the electron transfer is slowed down and the so called Marcus inverted region is reached.<sup>[62]</sup>

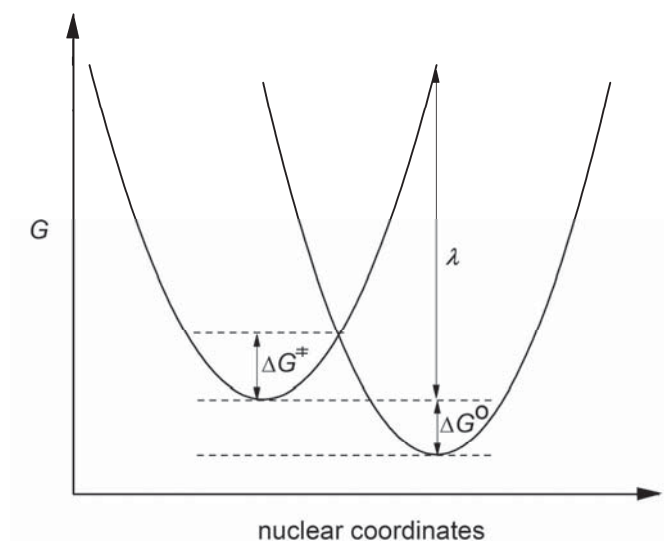
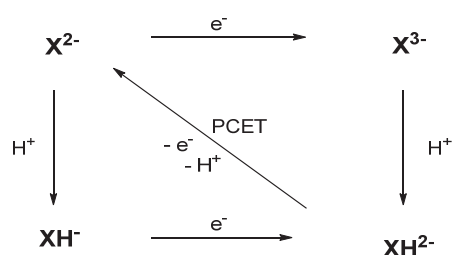


**Figure 1.2:** Paraboloids of the free energy surface of the educt and product of an electron transfer reaction and relation to thermodynamic parameters.<sup>[64]</sup>

More recently, it has been shown that a Marcus Theory type description is also applicable to proton coupled electron transfer (PCET) reactions.<sup>[65–67]</sup> In the broadest sense, a PCET reaction is any reaction, in which an equal number of protons and electrons are transferred. PCET is ubiquitous in biological systems and essential in processes such as photosynthesis, in the respiratory chain, and during water oxidation.<sup>[68]</sup> It may also play a role in several processes present in solar fuel cells.<sup>[68]</sup> A concerted proton and electron transfer in metalloenzymes was first proposed by Stiefel, who described mechanistic scenarios of molybdenum enzymes in 1973.<sup>[69]</sup> A PCET process is often rationalized based on a thermodynamic square scheme (Scheme 1.2). Therein, the protonation step is described by the  $pK_a$  value, which can be determined *via* titration experiments for example. The electron transfer step is characterized by the  $E_{1/2}$  value of the corresponding redox couple, *i.e.* from the peak potentials as  $(E_{\text{red}}+E_{\text{ox}})/2$  determined *via* cyclic voltammetry (CV).



**Scheme 1.2:** Thermodynamic square scheme relating protonation, reduction and PCET in a dianionic compound  $X^{2-}$ .<sup>[64]</sup>

The overall proton and electron transfer reaction can proceed in a stepwise fashion, *i.e.* moving along the edges of the square scheme or in a concerted manner moving across the diagonal of the square scheme. If the reaction proceeds in a concerted mechanism without a discrete intermediate it is usually referred to as CPET (concerted proton and electron transfer). If the proton and electron are delivered to a single acceptor, the reaction is called HAT (hydrogen atom transfer). However, a clear distinction between CPET and HAT is not always possible.<sup>[70]</sup> A concerted mechanism is implied when the kinetic barrier of the PCET reaction, which can be derived from an Eyring plot, is smaller than the free energy differences associated with an initial PT or an initial ET step. Because of the uncertainties associated with values obtained from kinetic studies, the activation barrier should be at least several  $\text{kcal mol}^{-1}$  lower than the free energy barriers for the stepwise reactions, to draw reliable mechanistic conclusions.<sup>[70]</sup> The free energy change for the separate ET step ( $\Delta G^\circ_{\text{ET}}$ ) can be calculated according to (wherein  $F = 96485 \text{ C mol}^{-1}$ ):

$$\Delta G^\circ_{\text{ET}} = -F \cdot \Delta E^\circ = - (96.48 \text{ kJ mol}^{-1} \text{ V}^{-1}) \Delta E^\circ$$

The free energy change for the separate PT step ( $\Delta G^\circ_{\text{PT}}$ ) can be calculated according to ( $R = 8.314 \text{ J mol}^{-1} \text{ K}^{-1}$ ):

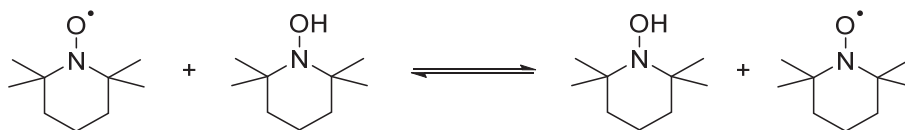
$$\Delta G^{\circ}_{\text{PT}} = -RT \ln(pK_a)$$

The bond dissociation free energy (BDFE) is directly connected to the free energy of the reaction and can be calculated as:<sup>[64]</sup>

$$\text{BDFE}_{\text{X-H}} (\text{kcal/mol}) = 1.37 \text{ p}K_a + 23.06 E_{1/2} + C_{\text{G,sol}}$$

The constant  $C_{\text{G,sol}}$  describes the free energy of the formation and solvation of  $\text{H}\cdot$ , and was reported as 54.9 in MeCN. The overall driving force of a PCET reaction, in which  $\text{H}^+$  and  $\text{e}^-$  are transferred from one reaction partner to the other can then be calculated from the difference of BDFEs between the two reaction partners.<sup>[64]</sup>

One typical PCET reagent for which proton and electron transfer occur in a concerted mechanism rather than in a stepwise fashion is 2,2,6,6-tetramethylpiperidinyloxy (TEMPO). The self-exchange between TEMPO and TEMPOH occurs with an Eyring barrier of  $\Delta G^\ddagger = 16.5 \text{ kcal mol}^{-1}$  in MeCN<sup>[71]</sup> while the free energy differences are  $\Delta G^\circ = 60 \text{ kcal mol}^{-1}$  both for an initial PT or an initial ET step.<sup>[64]</sup> Other well studied PCET reagents include further hydroxylamines as well as phenols, hydroquinones and catechols.<sup>[64]</sup>



**Scheme 1.3:** Self-exchange reaction between TEMPO and TEMPOH.<sup>[72]</sup>

## 1.4 Alternative Ligands in Iron Sulfur Clusters

While the majority of iron sulfur clusters are ligated by four cysteine residues of the surrounding protein, a subset of  $[2\text{Fe}-2\text{S}]$  clusters with different ligands exist has been found.<sup>[73]</sup> The most commonly observed of those alternative ligands is histidine but in most cases the role of this alternative ligand is not fully understood yet. Roles of the alternative ligands may include tuning of redox properties, mediating proton coupled electron transfer (PCET), cluster transfer or release, and sensing.<sup>[73]</sup> Some prominent examples include  $\text{Cys}_2\text{His}_2$  ligated Rieske centers,<sup>[74]</sup>  $\text{Cys}_3\text{His}$  ligated clusters as can be found in mitoNEET proteins<sup>[75]</sup> and the  $\text{Cys}_3\text{Arg}$  ligated  $[2\text{Fe}-2\text{S}]$  cluster in biotin synthase<sup>[76]</sup> (Figure 1.3).

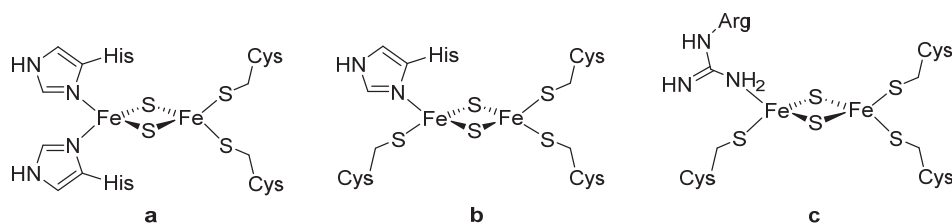


**Figure 1.3:** Coordination motifs of  $[2\text{Fe}-2\text{S}]$  clusters featuring alternative ligands *in vivo*: Rieske cofactors (a), mitoNEET proteins (b) and biotin synthase (c).

Of these examples, the Rieske center discovered in 1964 is the most thoroughly studied and its properties and function have been understood very well.<sup>[77]</sup> It features heteroleptic ligation with two histidine ligands on one of the iron centers and two cysteines on the other.<sup>[78–81]</sup> Rieske centers can be found in a multitude of electron transfer processes.<sup>[74]</sup> In respiratory and photosynthetic chains, they are responsible for the oxidation of quinole compounds in the Q-cycle, which is coupled to the generation of a proton gradient. It has been shown that the unpaired electron in the cluster's mixed valent form is located at the histidine coordinated iron site. The redox behavior of Rieske centers is strongly pH dependent, due to a coupling of the cluster's redox state to the protonation state of the histidine ligands.<sup>[78,81–86]</sup> This enables Rieske clusters to carry out PCET reactions during the conversion of hydroquinone substrates in the Q-cycle.<sup>[29]</sup>

The  $[2\text{Fe}-2\text{S}]$  cluster of mitoNEET proteins was discovered more recently in 2004 and was identified as a target for pioglitazone and thiazolidinedione drugs, which are used in the treatment of diabetes type 2.<sup>[75]</sup> Since they play a role in a number of processes related to human diseases, including proliferation of breast cancer and diabetes, the exact function of mitoNEET proteins is of special interest.<sup>[87–89]</sup> They contain a redox active and acid labile  $[2\text{Fe}-2\text{S}]$  cluster which features coordination by two cysteines on one of the iron centers and by one cysteine and one histidine on the other.<sup>[90–95]</sup> Several functions for this cluster have been proposed including redox and/or pH sensing,<sup>[96]</sup> cluster-transfer<sup>[97]</sup> and mediating redox reactions.<sup>[94]</sup> The exact function of the cluster and the role of the unique single histidine ligand have not been fully understood to date. The backside of the histidine's imidazole moiety is positioned at the surface of the protein and is thus easily exposed to changes in the environment of the protein.<sup>[93]</sup> The histidine has thus been proposed to act as a proton responsive ligand and indeed the mitoNEET  $[2\text{Fe}-2\text{S}]$  cluster shows a pH dependent redox potential.<sup>[75,98]</sup> Pulsed EPR studies have confirmed that the unpaired electron is localized on the histidine ligated iron site in the cluster's mixed valent form and reduction of the cluster was shown to be coupled to proton uptake.<sup>[99]</sup> Thus a role in PCET reactions similar to that of Rieske clusters has been proposed.<sup>[100]</sup> The redox state of the cluster is crucial in mediating the protein's reactivity. Transfer of the  $[2\text{Fe}-2\text{S}]$  cluster from mitoNEET to an acceptor protein can only occur in the diferric state while no cluster transfer has been observed in the

mixed valent form.<sup>[101]</sup> Histidine ligation was shown to be essential for this process, since no cluster transfer was observed in mutants lacking this residue.<sup>[102]</sup>

The mitoNEET [2Fe–2S] cluster is embedded in a network of hydrogen bonding residues, which are conserved throughout the protein family namely Lys55, Ser77, and Asp84 (Figure 1.4).<sup>[96]</sup> These hydrogen bonds are essential in modulating both the stability of the cluster and the functionality of the protein. They may also act as a gateway for protons during PCET reactions. Other [2Fe–2S] clusters featuring a Cys<sub>3</sub>His ligation include the bacterial transcription factor IscR which modulates the binding of DNA and glutaredoxines, which are responsible for ATF1 binding.<sup>[73]</sup>

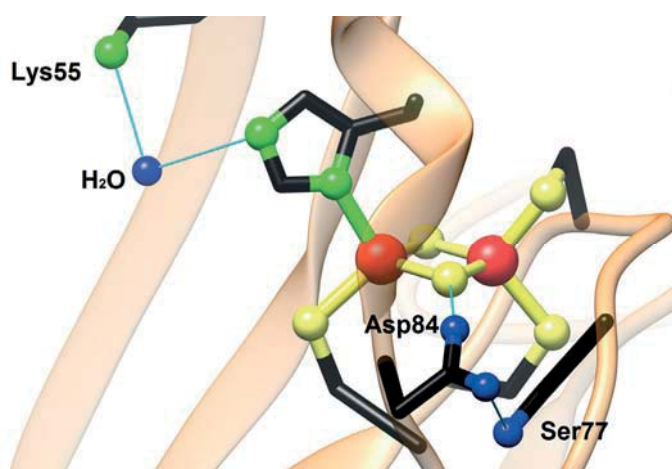
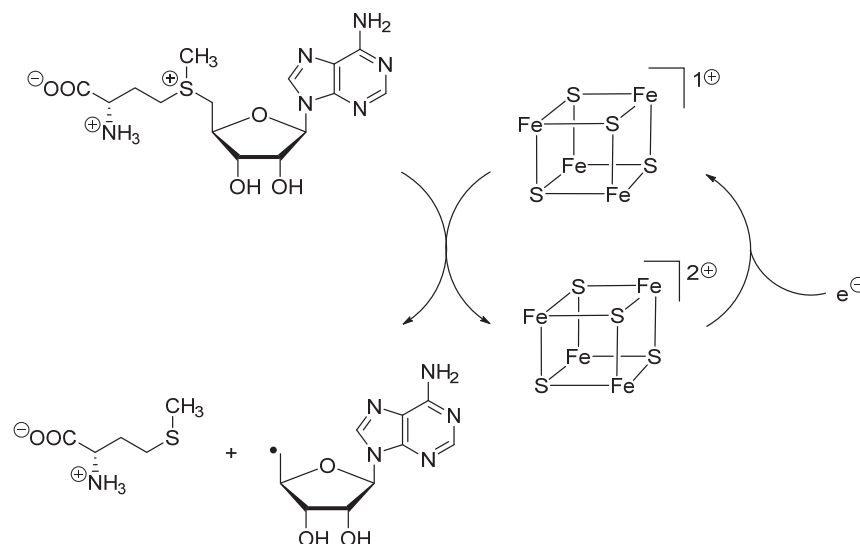


**Figure 1.4:** The [2Fe–2S] cluster of human mitoNEET protein (PDB entry 2QH7) in a network of hydrogen bonds with the conserved residues Lys55, Ser77, Asp84, and one molecule of water.<sup>[96]</sup> Color code: Fe (red), S (yellow), N (green), O (blue), C (black).

## 1.5 Iron Sulfur Clusters in Radical SAM Enzymes

All of the more than 600 enzymes in the radical SAM family mediate radical reactions by using *S*-adenosyl-*L*-methionine (SAM), which has been referred to as the “poor man’s adenosylcobalamin” because of its versatility,<sup>[103]</sup> and which can reductively be cleaved into methionine and a 5′-deoxyadenosyl (5′-doA) radical.<sup>[104–107]</sup> This radical is a potent oxidant and can abstract an H atom from the respective substrate, thus initiating substrate conversion (Scheme 1.4). All members of the radical SAM family share a [4Fe–4S] cluster coordinated by the cysteine residues of a conserved CX<sub>3</sub>CX<sub>2</sub>C motif.<sup>[106]</sup> SAM can bind to a free coordination site of this cluster in a bidentate fashion *via* its carboxylate and amino functions.<sup>[108]</sup> During turnover, the [4Fe–4S] cluster is oxidized and must be re-reduced before a second equivalent of SAM can be cleaved into methionine and 5′-doA.<sup>[109]</sup> This conserved [4Fe–4S] cluster is both crucial in delivering an electron to SAM to initiate bond

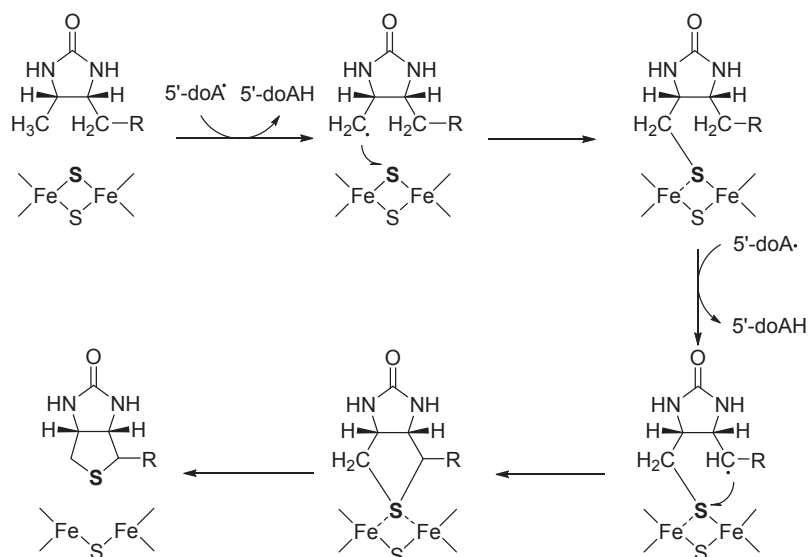
cleavage but also in positioning SAM in close proximity to the respective substrate and thus facilitating the subsequent H atom abstraction.<sup>[108]</sup> A subset of radical SAM enzymes contain so called auxiliary iron sulfur clusters. Prominent examples for this group are the two sulfur donating enzymes biotin synthase (BioB) and lipoyl synthase (LipA) as well as methylthiotransferases MiaB and RimO.<sup>[107]</sup>



**Scheme 1.4:** Radical generation from SAM mediated by a [4Fe-4S] cluster.<sup>[107]</sup>

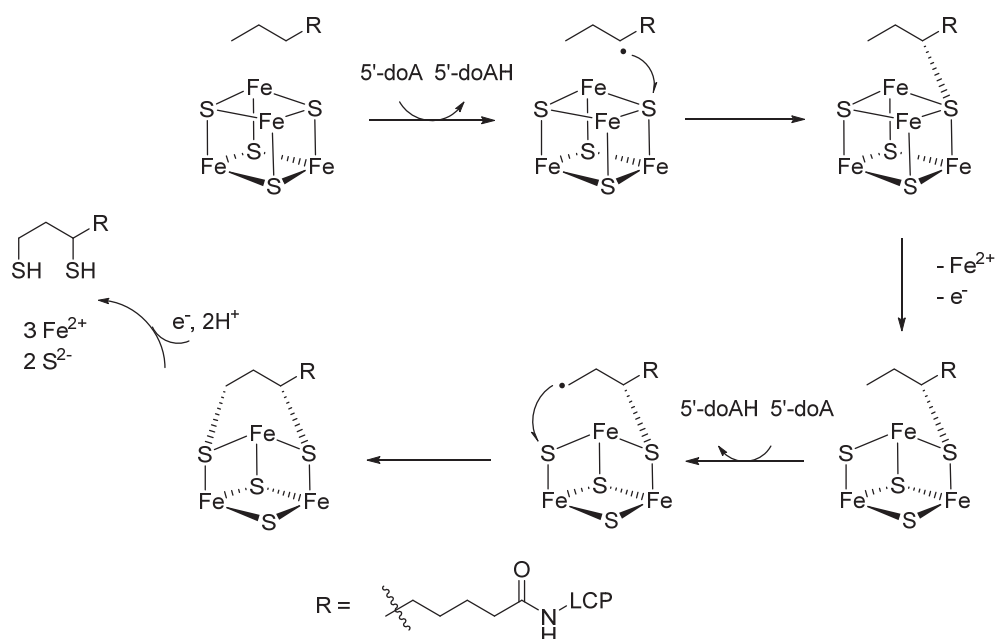
Biotin synthase (BioB) is arguably the most prominent example of a radical SAM enzyme. It catalyzes the final step of biotin biosynthesis by inserting a sulfur atom into dethiobiotin (DTB) thus closing the heterocycle of this natural product. Two equivalents of 5'-doA, *i.e.* two equivalents of SAM, are required to activate DTB in positions C6 and C9. BioB contains the conserved [4Fe-4S] cluster needed to achieve radical initiation and an auxiliary [2Fe-2S] cluster, whose role has been subject to intensive debates and is now believed to be the sulfur source of the catalyzed reaction.<sup>[110-114]</sup> The crystal structure of BioB reported in 2004 shows the substrate (DTB) placed between the [2Fe-2S] and the [4Fe-4S] cluster.<sup>[115]</sup> Reduction of the auxiliary [2Fe-2S] cluster during turnover was observed *via* EPR spectroscopy, indicating attack of an organic radical to this cluster.<sup>[116]</sup> Further evidence for a role of the [2Fe-2S] cluster as sulfur donor was provided by studies of biotin synthase reconstituted to contain a [2Fe-2Se] cluster which was shown to produce selenobiotin from dethiobiotin.<sup>[117]</sup> Based upon these findings, the following mechanism for the reaction catalyzed by BioB has been proposed (Scheme 1.5).<sup>[118]</sup> The 5'-doA radical produced from SAM abstracts an H atom from DTB resulting in the formation of a highly reactive primary radical. This radical attacks the bridging sulfide of the [2Fe-2S] cluster and forms the first C-S bond. A second 5'-doA radical then abstracts a second H atom from DTB and subsequently a second radical attack on the bridging sulfide can occur. After formation of the second C-S bond, biotin can

be released as a final product. During this process, the [2Fe–2S] cluster loses one of its bridging sulfides and must be reconstituted before a second turnover can take place.<sup>[118]</sup> BioB is thus often called a “suicide enzyme”.<sup>[30]</sup>



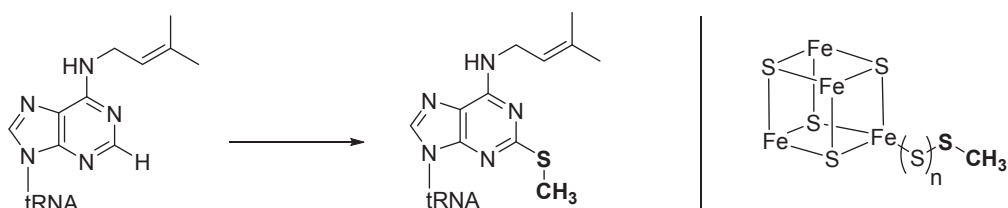
**Scheme 1.5:** Postulated mechanism for biotin biosynthesis as achieved by BioB.<sup>[118]</sup>

Similar to BioB, lipoyl synthase LipA achieves the formation of two C–S bonds on an octanoyl chain attached to a lipoyl carrier protein (LCP).<sup>[119]</sup> The crystallographic characterization reported in 2014 showed two independent [4Fe–4S] clusters.<sup>[120,121]</sup> One of them is coordinated by three cysteine residues of the conserved CX<sub>3</sub>CX<sub>2</sub>C motif and is responsible for radical generation from SAM. The second [4Fe–4S] cluster is coordinated by three cysteine ligands and one serine ligand and acts as an auxiliary cluster similar to the auxiliary [2Fe–2S] cluster in BioB. Two equivalents of SAM are needed for one turnover as two C–S bonds are formed in a stepwise mechanism (Scheme 1.6).<sup>[122]</sup> Evidence for a crosslinked enzyme-substrate intermediate was reported in 2014 relying on EPR and Mößbauer spectroscopy. It was found that the [4Fe–4S] cluster loses the serine-coordinated iron ion during the formation of this intermediate, which shows the spectroscopic characteristics of a [3Fe–4S]<sup>0</sup> cluster with an  $S = 1/2$  ground state.<sup>[123]</sup> This [3Fe–4S] intermediate was also characterized crystallographically.<sup>[122,124]</sup> The auxiliary cluster is sacrificed during turnover and has to be regenerated. Thus LipA can be regarded a suicide enzyme similar to BioB.<sup>[125]</sup> Mößbauer spectroscopy revealed, that only the second [4Fe–4S] cluster which is used for radical generation remains present in the enzyme after turnover.<sup>[123]</sup>



**Scheme 1.6:** Formation of two C–S bonds on an octanoyl chain catalyzed by lipoyl synthase *via* a cross linked intermediate.<sup>[122,124]</sup>

A second type of sulfur donating radical SAM enzymes featuring auxiliary iron sulfur clusters are methylthiotransferases such as MiaB and RimO.<sup>[107,126,127]</sup> Similar to LipA, both MiaB and RimO harbor two distinct [4Fe–4S] clusters. MiaB catalyzes the methylthiolation of an adenosine nucleotide of tRNA (Scheme 1.7).<sup>[128]</sup> Similar to the reactions catalyzed by BioB and LipA, this requires the formation of a C–S bond, the H atom is abstracted from an  $sp^2$  hybridized carbon instead of from an  $sp^3$  hybridized carbon. Similar to MiaB, RimO catalyzes a methylthiolation, but in this case of an  $sp^3$  hybridized carbon of a conserved aspartate in ribosomal protein S12 in *Escherichia coli*.<sup>[129]</sup>



**Scheme 1.7:** Methylthiolation of an adenosine nucleotide of tRNA catalyzed by MiaB (left) *via* an intermediate [4Fe–4S] methyl carrier (right).

The main difference between methylthiotransferases and sulfur insertion enzymes BioB and LipA lies in their use of SAM. While BioB and LipA cleave two equivalents of SAM to generate two equivalents of 5'-doA, methylthiotransferases cleave one equivalent of SAM to generate 5'-doA but the second equivalent of SAM is used as the methyl donor.<sup>[128,130]</sup> One plausible mechanistic scenario involves the generation of a protein bound methylthio group



which is subsequently transferred to the substrate.<sup>[107]</sup> This hypothesis is supported by studies by Landgraf *et al.*, who have identified the protein bound methylthio intermediate (Scheme 1.7) and performed labeling studies showing that it is chemically competent in transferring its methylthio group to the respective substrates.<sup>[131]</sup>

### 1.6 Synthesis and Reactivity of Biomimetic Iron Sulfur Complexes

Since the discovery of their biological blueprints in the 1960s, synthetic iron sulfur clusters have largely contributed to the understanding of their structure, spectroscopic features and reactivity, and have been essential in establishing relations between structural and spectroscopic signatures.<sup>[132–134]</sup> In comparison with their biological blueprints, most synthetic iron sulfur clusters display far lower redox potentials and can only be studied in organic solvents such as MeCN.<sup>[132]</sup> They are mostly very sensitive toward the presence of oxygen and water, due to the lability of the bridging sulfides. The first synthetic [2Fe–2S] cluster **1**<sup>2-</sup> reported in 1973 features bidentate chelating thiolate ligands and was also prepared in a self-assembly reaction using FeCl<sub>3</sub>, NaSH and the deprotonated ligand *o*-xylyl- $\alpha$ - $\alpha'$ -dithiol.<sup>[135]</sup> The simple tetrachloro-coordinated cluster **2**<sup>2-</sup> is readily available from a self-assembly reaction using [FeCl<sub>4</sub>](NEt<sub>4</sub>)<sub>2</sub> and (SiMe<sub>3</sub>)<sub>2</sub>S with almost quantitative yields and has been used as a precursor in the synthesis of a number of biomimetic [2Fe–2S] clusters.<sup>[132,136,137]</sup> One example is the synthetic [2Fe–2S] cluster **3**<sup>2-</sup> reported in 2008, which is coordinated by thiolate ligands as well.<sup>[138]</sup> Through secondary bonding interactions, a five coordination of both ferric ions was achieved, which may present a model for transition states of biological conversions occurring on [2Fe–2S] clusters.

While the naturally occurring cysteine ligands have been mimicked by use of thiolate ligands in synthetic iron sulfur cluster chemistry, varying approaches for modeling the N-donor of the histidine ligands have been reported. Benzimidazole based ligands have been used by Beardwood and Gibson in the synthesis of homoleptic [2Fe–2S] clusters starting from precursor **2**<sup>2-</sup> in a simple ligand exchange reaction.<sup>[139]</sup> Among these are clusters **4**<sup>2-</sup> and **5**<sup>2-</sup> which feature mixed S/N or O/N ligation on both iron sites. The first neutral [2Fe–2S] cluster **6** was reported by Tatsumi in 2005 and features terminal monodentate amide ligands.<sup>[140]</sup> Due to its neutral charge it is soluble in a broad range of solvents and makes a multitude of reactivity studies possible. A different approach in mimicking N-donating ligands is the use of ketimate ligands such as in neutral cluster **7** reported by Holland and neutral cluster **8** reported by Driess.<sup>[141,142]</sup> In both cases the synthesis of these clusters relied on the conversion of mononuclear iron(I) species with elemental sulfur to achieve sulfide insertion as the last step of cluster synthesis. Both species have also been isolated and structurally

characterized in their mixed valent forms and an extensive delocalization was observed in **8** via Mößbauer spectroscopy. Iron(I) precursors have also been used in the synthesis of  $[2\text{Fe}-2\text{E}]$  clusters **9a-c** ( $\text{E} = \text{O}, \text{S}, \text{Se}$ ) by reaction with molecular oxygen, elemental sulfur or selenium.<sup>[143]</sup> These neutral diferric compounds feature bidentate N-donating capping ligands and a distorted square planar coordination of the iron centers has been observed in the  $[2\text{Fe}-2\text{O}]$  species, whereas the  $[2\text{Fe}-2\text{S}]$  and  $[2\text{Fe}-2\text{Se}]$  species show a tetrahedral coordination of the iron centers.

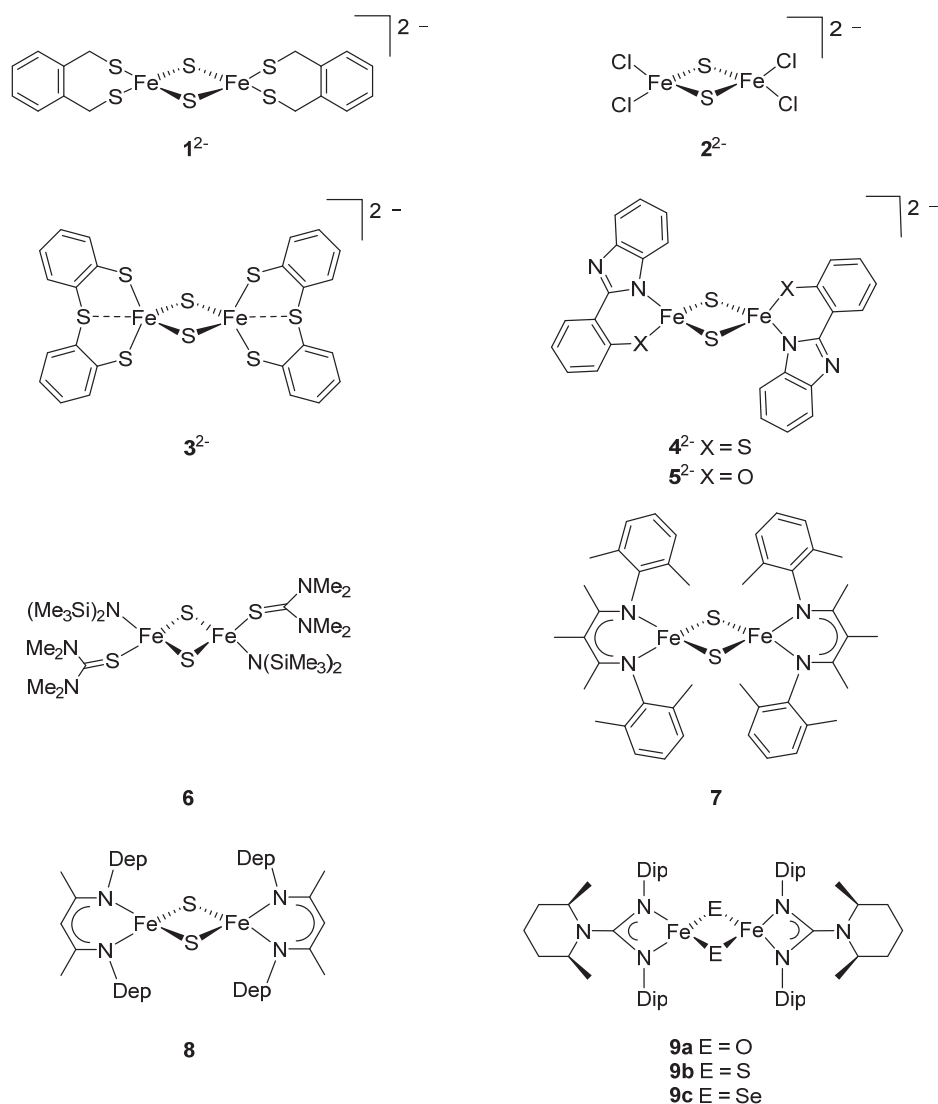


**Figure 1.5:** Synthetic  $[2\text{Fe}-2\text{S}]$  clusters: The first synthetic  $[2\text{Fe}-2\text{S}]$  cluster  $1^{2-}$ , tetrachloro-coordinated cluster  $2^{2-}$  serving as a precursor for new synthetic model systems, thiolate ligated cluster  $3^{2-}$  featuring five-coordinate iron centers, benzimidazole based clusters  $4^{2-}$  and  $5^{2-}$ , neutral cluster **6** and ketimine ligated clusters **7** and **8** (Dep =  $\text{C}_6\text{H}_3\text{Et}_2$ ) illustrating various approaches in mimicking the naturally occurring histidine ligand and chalcogene analogues of  $[2\text{Fe}-2\text{S}]$  clusters **9a-c** (Dip =  $\text{C}_6\text{H}_3\text{Pr}_2$ ).

While a number of homoleptic [2Fe–2S] clusters have been prepared *via* different synthetic strategies, the synthesis of heteroleptic [2Fe–2S] clusters is considerably more challenging, since ligand scrambling and formation of homoleptic side products have to be suppressed.

The first synthetic analogue **11**<sup>2-</sup> mimicking the heteroleptic {N<sub>2</sub>} {S<sub>2</sub>} coordination found in Rieske proteins was only reported in 2008 (Figure 1.6).<sup>[144]</sup> This heteroleptic cluster can be viewed as a combination of all-N-ligated cluster **10**<sup>2-</sup> and all-thiolate ligated cluster **1**<sup>2-</sup> and was prepared in a stepwise ligand exchange reaction starting from precursor **2**<sup>2-</sup>. The average *g* value of *g*<sub>av</sub> = 1.92 found in the mixed valent form is in good agreement with the *g*<sub>av</sub> found in Rieske Proteins (about 1.90–1.91).<sup>[77,145,146]</sup>

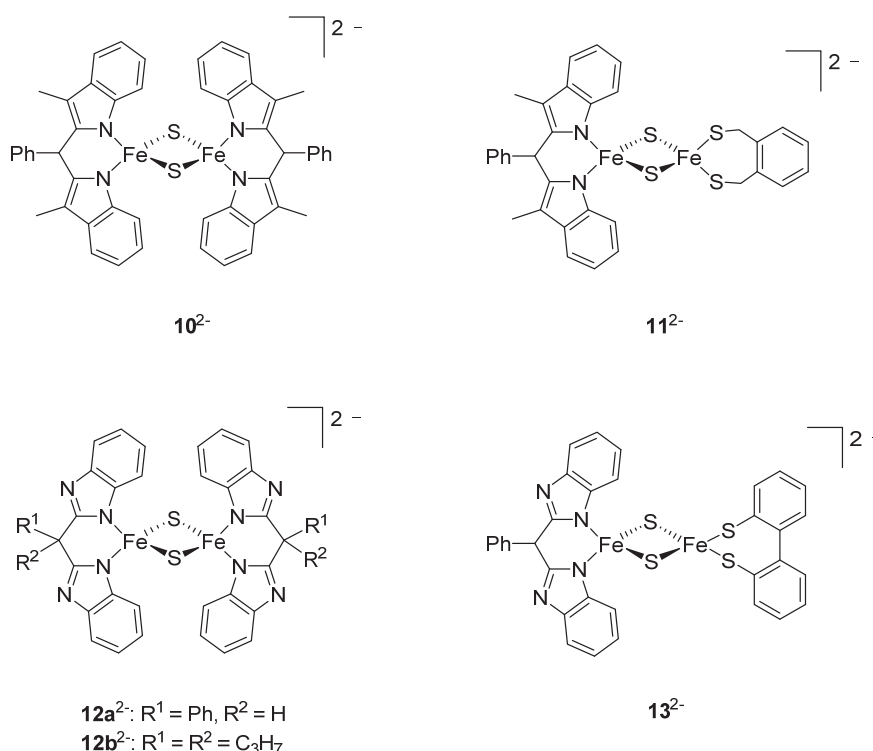
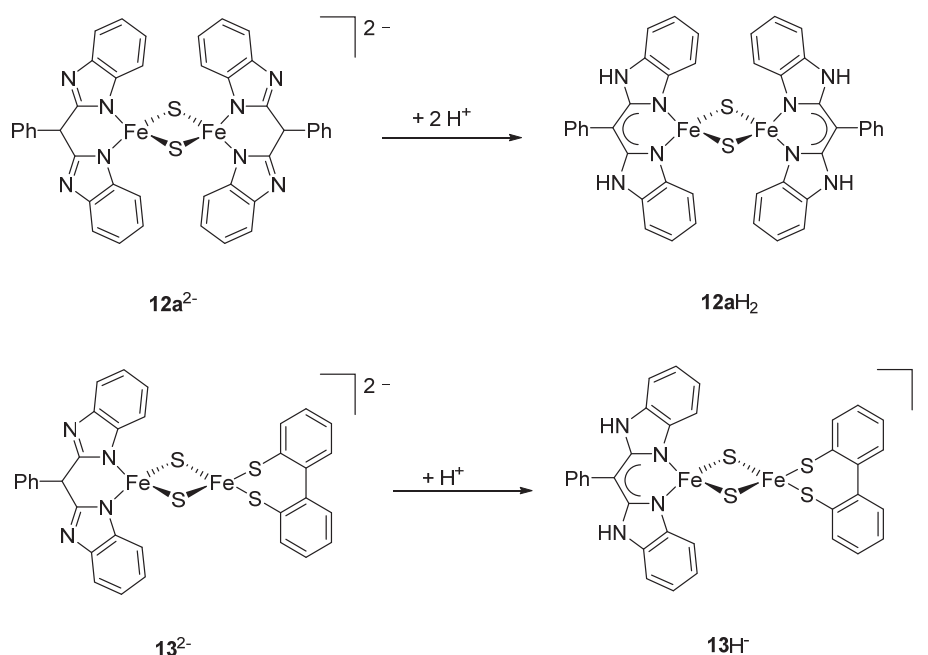


**Figure 1.6:** Evolution of synthetic models for [2Fe–2S] Rieske centers from 2008 to 2014.<sup>[144,147,148]</sup>

Although **10**<sup>2-</sup> proved to be a good structural and spectroscopic model, it lacks a distal N-atom in the ligand's backbone to fully emulate the properties of the histidine as a proton responsive ligand. To enable protonation and thus proton coupled electron transfer (PCET), bis-benzimidazoles were used as ligands and clusters **12**<sup>2-</sup> and **13**<sup>2-</sup> were prepared.<sup>[147–149]</sup>

The bis-thiolate ligand was modified from *o*-xylyl- $\alpha$ - $\alpha'$ -dithiol to 2,2-dithio-1,1-biphenyl in order to improve crystallization properties. The second generation Rieske model **13**<sup>2-</sup> is a high fidelity model that does not only mimic the structural and spectroscopic but also the functional properties of Rieske [2Fe–2S] clusters. The diferric forms of both homoleptic cluster **12a**<sup>2-</sup> and heteroleptic cluster **13**<sup>2-</sup> was shown to undergo tautomerization upon protonation of the N-atoms in the backbone of the benzimidazole-type terminal ligands to

form the fully conjugated ligand system (Scheme 1.8). This tautomerization led to rise of an intense band in the visible absorption spectra of these compounds ( $\lambda_{\max} = 386 \text{ nm}$ ,  $\varepsilon = 60000 \text{ M}^{-1} \text{ cm}^{-1}$  for **12aH<sub>2</sub>** and  $\lambda_{\max} = 385 \text{ nm}$  and  $\varepsilon = 47000 \text{ M}^{-1} \text{ cm}^{-1}$  for **13H<sup>-</sup>**).<sup>[147,148]</sup> No tautomerization was observed upon protonation of the respective mixed valent species **12a<sup>3-</sup>** and **13<sup>3-</sup>**.



**Scheme 1.8:** Tautomerization observed upon protonation of the benzimidazole-based terminal ligands in diferric clusters **12a<sup>2-</sup>** and **13<sup>2-</sup>**.<sup>[147,148]</sup>

The ability to undergo PCET reactions was demonstrated for **13<sup>2-</sup>** and also for homoleptic models **12a<sup>2-</sup>** and **12b<sup>2-</sup>** and the respective square schemes have been established for **13<sup>2-</sup>** and **12b<sup>2-</sup>**.<sup>[148,150]</sup> In case of **12a<sup>2-</sup>**, all studies had to be carried out in DMF due to solubility issues. Since the  $\text{p}K_{\text{a}}$  values of acids used for protonation are not well defined in DMF, this prevented the summary in a reliable square scheme. Self-exchange between diferric **12b<sup>2-</sup>** and mixed valent **12b<sup>3-</sup>** was monitored by <sup>1</sup>H NMR spectroscopy. Since both species show distinct resonances in <sup>1</sup>H NMR spectra, self-exchange is slow on the NMR time scale and a line shape analysis in mixtures containing varying amount of **12b<sup>2-</sup>** and **12b<sup>3-</sup>** allowed for the determination of a free energy barrier of  $10.5 \text{ kcal mol}^{-1}$ .<sup>[151]</sup> In contrast to electron transfer, proton transfer, *i.e.* self-exchange between the protonated and unprotonated cluster, is fast on the NMR time scale.<sup>[151]</sup> Additionally, **12a<sup>4-</sup>** was the first example of a fully characterized all-ferrous [2Fe–2S] cluster.<sup>[152]</sup>